



# Analytical calculations and Monte-Carlo simulations of a high-resolution backscattering spectrometer for the long wavelength target station at the Spallation neutron source

H.N. Bordallo<sup>a,\*</sup>, K.W. Herwig<sup>b,2</sup>, G. Zsigmond<sup>c</sup>

<sup>a</sup>Intense Pulsed Neutron Source, Argonne National Laboratory, Argonne, IL 60439, USA

<sup>b</sup>Spallation Neutron Source, Oak Ridge National Laboratory, Oak Ridge, TN 37831, USA

<sup>c</sup>Hahn–Meitner-Institut, SFI, Glienicker Strasse 100, D-14109 Berlin, Germany

Received 30 April 2002; received in revised form 29 May 2002; accepted 4 June 2002

## Abstract

Using the Monte-Carlo simulation programs McStas and VITESS, we present the design principles of the proposed high-resolution inverse geometry spectrometer on the Spallation neutron source (SNS)—long wavelength target station (LWTS). LWTS will enable the combination of large energy and momentum transfer ranges with energy resolution. Indeed the resolution of this spectrometer lie between that routinely achieved by spin echo techniques and the design goal of the high-power target station (HPTS) backscattering spectrometer. This niche of energy resolution is interesting for the study of slow motions of large objects and we are led to the domain of large molecules—polymers and biological molecules.

© 2002 Elsevier Science B.V. All rights reserved.

PACS: 07.05.Tp; 29.30.Hs; 29.25.Dz

Keywords: Neutron instruments; Backscattering; Monte Carlo simulation packages

## 1. Introduction

The concept of the inverse geometry spectrometer came about with the plans to build a long

wavelength target station (LWTS) at SNS [1], which will provide high flux of long-wavelength neutrons. The actual instrument design employs mica analyzers close to backscattering geometry (final neutron wavelength of 20 Å), with an extremely high-energy resolution ( $\delta\omega \leq 0.2 \mu\text{eV}$  FWHM, elastic).

Using analytical calculations the general instrument design and instrumental resolution were obtained. Then, in order to optimize the layout of individual components and to estimate the instrument performance, the Monte-Carlo

\*Corresponding author. Present address: Hahn–Meitner-Institute, SFI, Glienicker Strasse 100, D-14109 Berlin, Germany. Tel.: +49-30-8062-3174; fax: +49-30-8062-3094.

E-mail address: bordallo@hmi.de (H.N. Bordallo).

<sup>1</sup>Work supported by the U.S. DOE-BES Contract No W-31-109-Eng-38.

<sup>2</sup>Work supported by the U.S. DOE Contract No. DE-AC05-96OR22464.

simulation programs McStas and VITESS (Virtual Instrumentation Tool for ESS) [2–4], developed, respectively, at Risø National Laboratory and Hahn–Meitner-Institut, have been used. McStas and VITESS offer a general framework to compose virtual neutron scattering instruments and supports both reactors and spallation sources. Comparing the simulations results obtained using both packages allows to take advantage of the strength of each program separately, and also check for any possible inaccuracy of the final results.

## 2. Description of the instrument

### 2.1. The basic design

Consider that the uncertainty in the energy transfer for an inverted-geometry spectrometer using crystal analyzers can be separated into a term dependent on the primary spectrometer ( $\delta\omega_P$ , components before the sample) and on a term dependent on the secondary spectrometer ( $\delta\omega_S$ , components after and including the sample). And taking the approximation that the terms are independent and that the uncertainties add in quadrature the energy resolution function is given by Ref. [5],

$$\delta\omega = \sqrt{(\delta\omega_P)^2 + (\delta\omega_S)^2} \quad (1)$$

where

$$\delta\omega_P = 2E_i \sqrt{\left(\frac{\delta L_i}{L_i}\right)^2 + \left(\frac{\delta t_0}{t_i}\right)^2} \quad (2)$$

and

$$\delta\omega_S = 2 \sqrt{E_i^2 \left(\frac{\delta t_f}{t_i}\right)^2 + E_i^2 \left[ (\cot(\theta_B)\delta\theta_B)^2 + \left(\frac{\delta d}{d}\right)^2 \right]^2} \quad (3)$$

where,  $E_i$  is the incident neutron energy,  $L_i$  is the moderator–sample distance,  $t_i$  is the incident neutron flight time,  $t_0$  is the emission time of the neutron from the moderator and  $t_f$  is the time for the neutron of known final energy to travel from the sample to analyzer to detector. On a crystal

analyzer spectrometer, the final neutron energy,  $E_f$ , is fixed by Bragg reflection from the analyzer crystals.

The first term in Eq. (2) is small compared to the second, and therefore the contribution from the primary spectrometer to the resolution arises from the moderator pulse width ( $\delta t_0$ ) at a given neutron energy. On the other hand, the contribution from the secondary spectrometer, Eq. (3), represents uncertainty in the lattice parameter ( $\delta d$ ) of the crystal analyzers and the uncertainty of the Bragg angle ( $\delta\theta_B$ ).  $\delta\theta_B$  has contributions both from the analyzer crystal mosaic and the sample dimensions.

Traditionally, the resolution contributions from the primary and secondary spectrometers are matched in an effort to optimize the count rate in the detectors for a given resolution. The decoupled poisoned solid methane moderator at LWTS generates a pulse with a width of 90  $\mu$ s for  $\lambda = 20$  Å. For a neutron  $\lambda$  of 20 Å the energy reflected from the (002) planes of mica is 0.2045 meV. In order to achieve the timing resolution necessary for the desired  $\delta\omega$ , the primary flight path of the spectrometer with a long initial guide section around 63 m from moderator to sample is required. For many reasons it is desirable to design the instrument with the analyzers slightly out of backscattering. In fact, this component of the resolution,  $\cot(\theta_B)\delta\theta_B$ , can be relaxed from exact backscattering, without modifying the overall resolution significantly [6]. A reasonable choice based on sample/detector geometry is to opt for a Bragg angle of 87.5°.

In contrast to spectrometers such as IRIS with lower resolution requirements, in this particular case the sample size can easily dominate the first and second terms in Eq. (3). Restricting the sample size is not an issue in case where only limited amount of sample is available, however, a restricted beam size lowers the neutron flux into the detector. Optimization of the secondary spectrometer requires to keep the first term of Eq. (3) small compared to the second. Constraining the design to a 2 m sample-analyzer flight path leads to an optimized sample size of 2 cm  $\times$  2 cm and a sample-size contribution to  $\delta\theta_B$  of 0.41°. The

total contribution of the sample size to Eq. (3) is 163 neV (to be added in quadrature to the  $\delta\theta_B$  contribution from the analyzer mosaic).

It is also important to understand the contributions to the  $Q$ -resolution for energy transfers near the elastic peak. In this case, the momentum transfer is given by

$$Q = \frac{4\pi \sin(\phi/2)}{\lambda_f} \quad (4)$$

where  $\phi$  is the angle between the incident neutron beam and the scattered beam. Differentiating the previous equation and considering that the uncertainty in  $\lambda_f$  is small, the uncertainty in  $Q$  is given by

$$\delta Q = \frac{4\pi}{\lambda_f} \cos\left(\frac{\phi}{2}\right) \left(\frac{\delta\phi}{2}\right). \quad (5)$$

The contributions to  $\delta\phi$  are the incident beam divergence  $\delta\phi_i$ , the contribution from sample size  $\delta\phi_s$  and the acceptance of the analyzer  $\delta\phi_a$ .

## 2.2. Details of the spectrometer design

In order to eliminate frame overlap at the sample position a disk chopper is located directly outside the target station. As LWTS operates at 10 Hz, the bandwidth chopper gives a wavelength band of 6.219 Å delivered to the sample at 63.36 m from the moderator. This wavelength band provides a range of energy transfers for the mica (002) reflection of  $\pm 60$  µeV. The performance characteristic of the instrument for near elastic scattering is as listed on Table 1.

Preliminary guide optimization was carried out by iteration of a Monte Carlo simulation. A curved guide 30 m long with radius of curvature of 1 km giving a characteristic wavelength of 7.9 Å with a critical angle equal to that of natural nickel was selected. Neutrons from the source were

biased into the guide entrance and the results were correspondingly normalized by the solid angle.

The following results as a function of moderator-guide distance, for a guide cross-section of 6 cm × 6 cm ending in a 6 m long natural nickel funnel with exit dimension of 2.4 cm × 2.4 cm, are represented in Fig. 1(a):

- (i)  $N_E$ , the number of neutrons exiting the guide (filled squares),
- (ii)  $N_S$ , the number of neutrons hitting the sample (half-filled squares) and
- (iii)  $r$ , ratio of neutrons hitting the sample to those exiting the guide (crosses).

Fig. 1(a) shows the effect of limiting the divergence of neutrons entering the guide. As the moderator-guide distance is increased, neutrons having a lower divergence enter the guide and a consequent lower divergence upon exiting the guide. In this case a higher percentage of exiting neutrons reach the sample. In an absolute sense, having the guide closer to the moderator results in a greater number of neutrons reaching the sample but a greater fraction of the exiting neutrons miss the sample and are potential source of background. Based on this assumption we choose a guide beginning at 8.34 m from the moderator accepting 20 Å neutrons with 0.5° divergence. The straight guide is made from sections of 1 m each, with a total length of 18.77 m.

Fig. 1(b) shows the performance obtained for a moderator-guide distance equal to 8.34 cm, ending in either a natural nickel or a super-mirror funnel with variable length and fixed exit dimension of 2 cm × 2 cm. We can clearly see that the number of neutrons that actually hit the sample is almost constant for a funnel length between 5 and 7 m, and that the use of a super-mirror coating will not improve this ratio. These results lead us to choose a funnel stopping 25 cm from the sample with a

Table 1  
Spectrometer performance for near elastic scattering

Analyzer crystal	$\lambda_f$ (Å)	$\delta\lambda_f$ (Å)	$\omega$ -range (µeV)	$\delta\omega$ (fwhm)(µeV)	$Q$ -range(Å) <sup>-1</sup>	$\delta Q$ (fwhm) (Å) <sup>-1</sup>
Mica (002)	20	6.219	−60 to 60	0.215	0.05 to 0.63	0.015 to 0.002
Mica (004)	10	6.219	−420 to 420	1.14	0.1 to 1.2	0.03 to 0.004

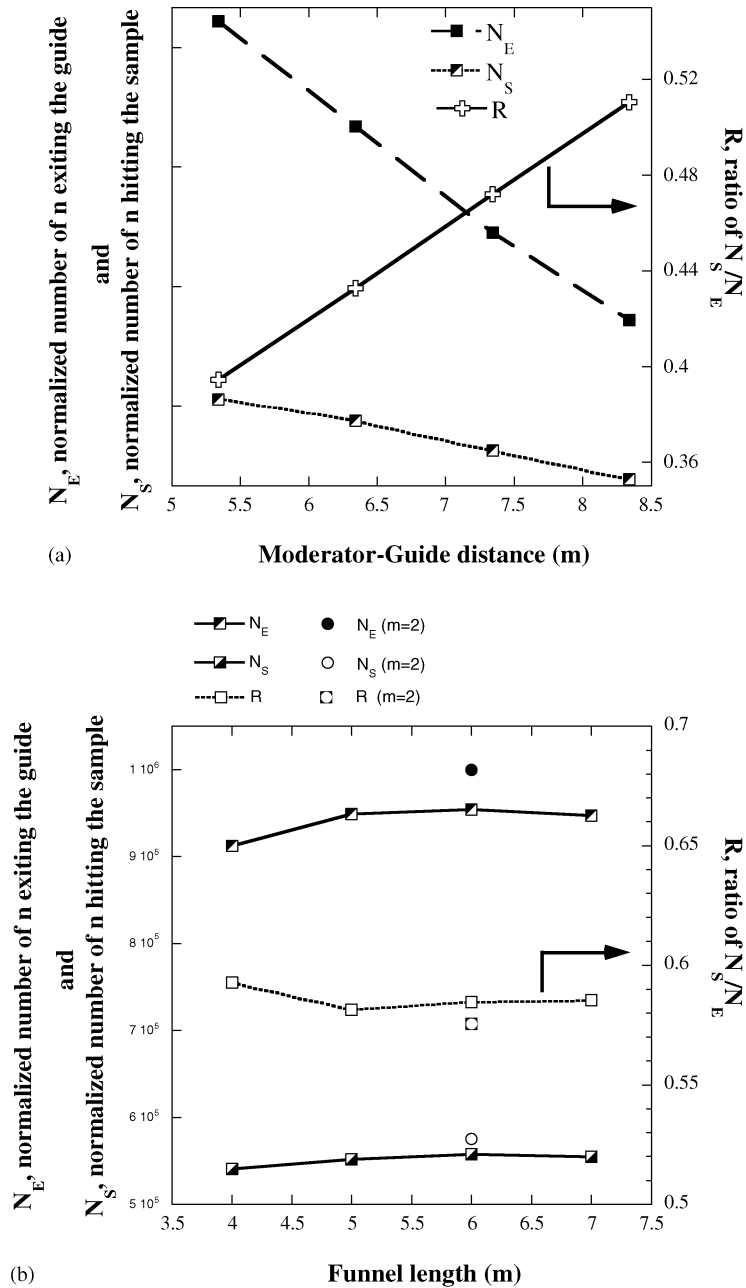


Fig. 1. Performance as a function of moderator-guide distance and funnel aperture, length and coating for a guide cross-section of 6 cm × 6 cm ending in a 6 m long nickel funnel. In Fig. 1(a) are represented  $N_E$ , the number of neutrons exiting the guide (filled squares),  $N_S$ , the number of neutrons hitting the sample (half-filled squares) and  $r$ , ratio of neutrons hitting the sample to those exiting the guide (crosses) for a fixed exit dimension of 2.4 cm × 2.4 cm. Fig. 1(b) shows the performance obtained for a moderator-guide distance equal to 8.34 cm, ending in either a natural nickel (squares) or a super-mirror (circles) funnel with variable length and fixed exit dimension of 2 cm × 2 cm.

length of 6 m and exit dimension of 2 cm × 2 cm. Total guide gains (ratio of neutrons on the sample with and without a guide) were estimated at 360 for  $\lambda = 20 \text{ \AA}$ . A description of the guide components is given on Table 2.

The mica analyzers are placed between 0° and 20° out of the scattering plane covering scattering angles from 5° to 160°, 2 m from the sample, and

have a mosaic spread estimated to be about 0.25° (fwhm). The detectors are approximately 175 cm from the analyzer crystals. Fig. 2 illustrates the scattering chamber design.

The peak count rate is expected to occur at the elastic peak. A typical case is when the total sample scattering is 10% of the incident beam flux. If elastic scattering dominates, the number of

Table 2  
Description of the instrument components

Component	Description	Characteristic
Moderator	Decoupled, 30 mm poisoned solid methane	$\delta t_0 = 90 \text{ \mu s}$ for $\lambda = 20 \text{ \AA}$
Analyzer crystal	Bragg angle d-spacing	87.5° mica (002)
Incident flight path	20 cm (H) × 15 cm (V) Guide/Funnel Moderator-guide distance	63.36 m from moderator to sample 8.34 m
Guide (cross section 6 cm)	Curved guide length Straight guide length Guide funnel length End of funnel—sample distance	30 m 18.77 m 6 m (natural Ni) 0.25 m
Sample	Geometry varied Sample-analyzer distance	2 × 2 cm <sup>2</sup> cross section of n beam 2 m

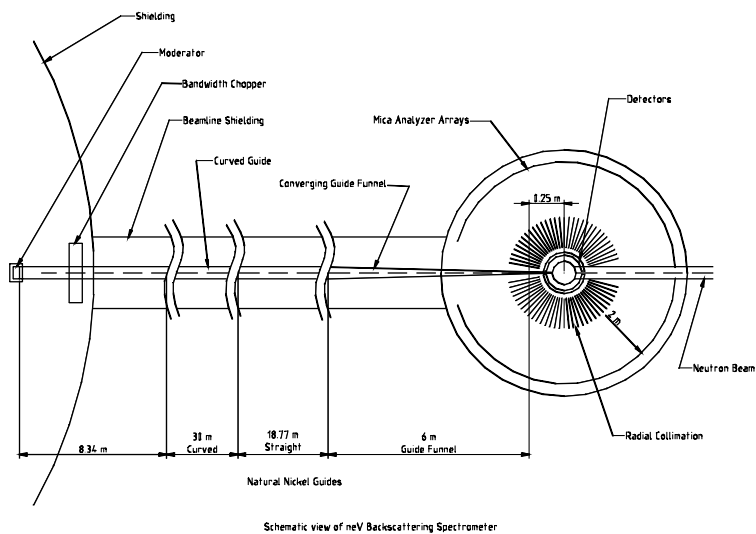


Fig. 2. Schematic view of the neV-backscattering at the LWTS at SNS.

neutrons scattered into the elastic peak is given by

$$N_s = F \times s \times \omega_R \times 0.1 \quad (6)$$

where  $F$  is the expected flux on the sample,  $s$  is the sample size and  $\omega_R$  is the resolution width of the primary spectrometer. For the mica high-resolution backscattering instrument at LWTS,  $F = 3.5 \cdot 10^4$  n/cm<sup>2</sup>-s- $\mu$ eV (2 MW, with a guide gain of 360),  $s$  is 4 cm<sup>2</sup> and  $\omega_R$  is 0.14  $\mu$ eV, making  $N_s = 1960$  n/s.

Each analyzer segment intercepts 1.85 sr of solid angle. Allowing a 20% loss for imperfect crystal reflectivity and loss due to mosaic spread, the number of neutrons intercepted by the detectors,  $F_D$ , is

$$F_D = \frac{3.7}{4\pi} \times N_s \times 0.8 = 462 \text{ n/s.} \quad (7)$$

An important figure of merit that should be estimated is the time required to obtain counts in the peak channel of the elastic peak for the 10% scattering sample:

$$t = P_T \times \frac{1}{F_D} \times N_Q \times \frac{N_R}{2} \quad (8)$$

where  $P_T$  is the desired number of counts,  $N_Q$  is the total number of single  $Q$ -point that gets summed into the detector and equal to 10 in this case,  $N_R$  is the number of bins across the elastic peak into which counts are stored, with a typical value of 20. The factor 2 corrects for the approximately triangular shape of the resolution function. As an example, the time required to obtain 4000 counts in the peak time channel is approximately 15 min. A similar analysis done for the performance of this instrument if it is built at the HPTS (high power target station operating at 60 Hz) at SNS shows a decrease in the performance of a factor of 4 in flux on sample. In addition, pulse suppression choppers would be required to eliminate intervening pulses with an attendant uncertainty in the background.

### 3. Monte Carlo resolution function

Of most interest is the resolution at the elastic peak. The simulation was performed using a cylindrical shell vanadium sample that only

scattered elastically. The sample was a 2 cm high hollow cylinder with an inner radius of 1.85 cm, an outer radius of 2.0 cm. In the McStas simulation, a total of 108 (or 216) crystal analyzers were used covering 3° in the horizontal plane (scattering plane) and 20° in the vertical plane. The crystals had dimensions approximately 2 cm  $\times$  2 cm (case 1) or 1 cm  $\times$  1 cm (case 2). Counts were collected using 3 position sensitive detectors, with 15 position channels each, (1 cm long channels along the length of the tube and 15 cm active length), infinitely thin, and 1 cm wide. The detectors were binned at 10  $\mu$ s time channels making possible a good line-shape analysis. On the other hand, in the VITESS simulation, 20 horizontal  $\times$  160 vertical (total 3200) analyzer elements were considered, each of size 0.2 cm  $\times$  0.5 cm  $\times$  0.5 cm. These see a 2.9° horizontal and 22.9° vertical angular range scattered by the sample.

Due to the sample/detector geometry ( $\theta_B = 87.5^\circ$ ), effects of optical aberration will be introduced. This appears as a wavelength variation of the analyzed neutrons or as a path-length difference between sample and detectors. In fact, if the analyzers sit on a Rowland circle a wavelength focusing can be achieved, on the other hand if the analyzers sit on a circle centered in the mid-point between the sample and the detector a practically constant path (an exact solution would be an ellipsoid) is obtained. Simulation carried out using VITESS shows that the approximate spherical geometry gives practically a constant wavelength selection as well (Fig. 3). For the simulations performed using McStas a combination of the two geometries was numerically generated with the analyzer crystals oriented symmetrically about either side of the detectors.

Fig. 4(a) shows the time/space distribution of elastically scattered neutrons across a central detector without the moderator obtained from the McStas simulations (case 1). A large time-of-flight contribution from the arrays of analyzer crystals is observed. This can be explained as follows. The central analyzer assembly illuminates the detector at the particular desired final lambda, while the adjacent ones illuminate it at plus or minus a slight lambda shift (due to the small change in Bragg angle), plus some flight path

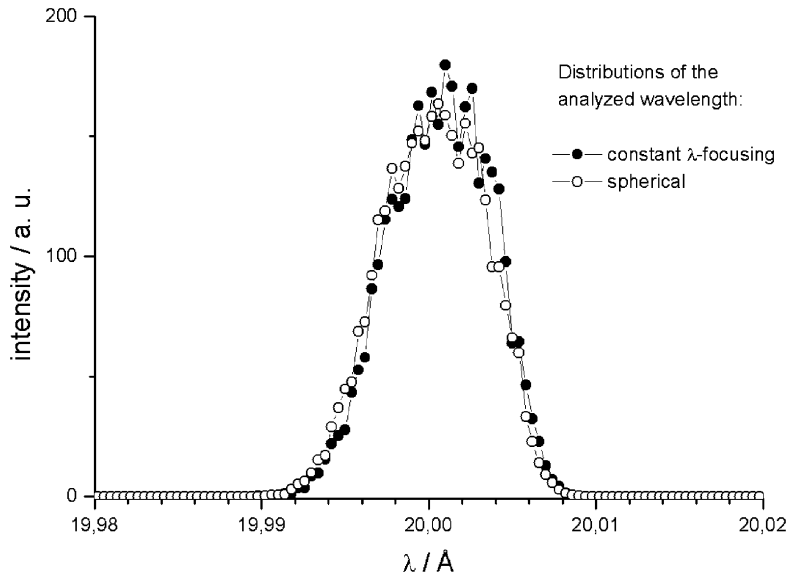


Fig. 3. Simulation carried out using VITESS shows that spherical geometry (constant secondary flight path length) gives practically a constant wavelength selection.

differences. When the analyzer arrays are this large ( $0.6^\circ$  apart), one actually sees the individual contributions of each analyzer assembly. This assumption is further confirmed by the simulation results shown in Fig. 4(b). In this case, when we subdivide the crystals into 1 cm wide ( $0.3^\circ$  apart, case 2) all the “stripes” seen in the previous figure have been removed. However, there is still a large time-of-flight contribution from the arrays of analyzer crystals. This is because the detector still “sees” a large change in the Bragg angle from the edges of the outlying crystals.

For the current target design, the moderator was modelled for both simulations as a combination of a Gaussian with an exponential decay in time [4]. A comparison of the results obtained from the two packages (Fig. 5) clearly shows that due to the tail on the moderator the resolution function is slightly asymmetric. Another observation is that on the energy loss side, the resolution function generated by McStas is broader compared to both analytical calculations and the results obtained by the VITESS simulation. This discrepancy can be explained by the geometrical arrangement and size (collimation) of the crystal analyzers. For geometries near back-scattering, a smaller optical aberration is observed

for the approximate spherical analyzer configuration (filled circles) because it decreases the secondary flight time differences relative to the exact wavelength focussing (open squares) as well as a combination of both geometries.

#### 4. Optimization of the instrument design

Improvements to the current design could include changing the moderator poison depth to a shallower position. This choice would improve the resolution but at a loss of flux on sample. A softer constraint on the instrument design is the initial flight path length. Because of the high transmission of the natural Ni guide, this distance can be increased without significantly changing the instantaneous flux on sample. Its sole effect would be to decrease the range of energy transfers accessible in a single frame measurement. This option could improve the resolution of the instrument by improving the resolution of the primary spectrometer. Other considerations include moving the spectrometer to a coupled moderator, and use a pulse-shaping chopper to modify the long time tail of the moderator pulse.

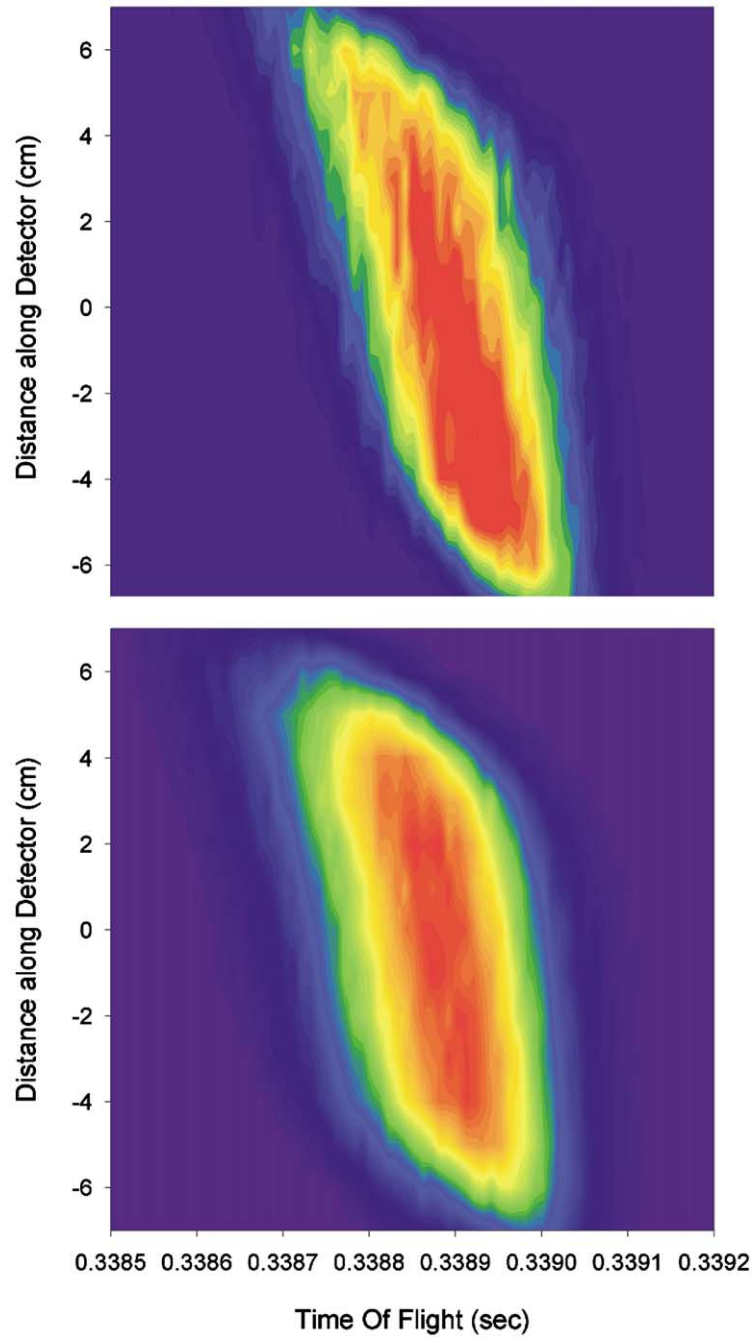


Fig. 4. Dispersion in ToF as a function of detector length without the moderator obtained from the McStas simulations. On (a) we show 2 cm wide crystals intercepting  $0.6^\circ$  as seen from the sample, and on (b) 1 cm wide crystals intercepting  $0.3^\circ$  as seen from the sample.

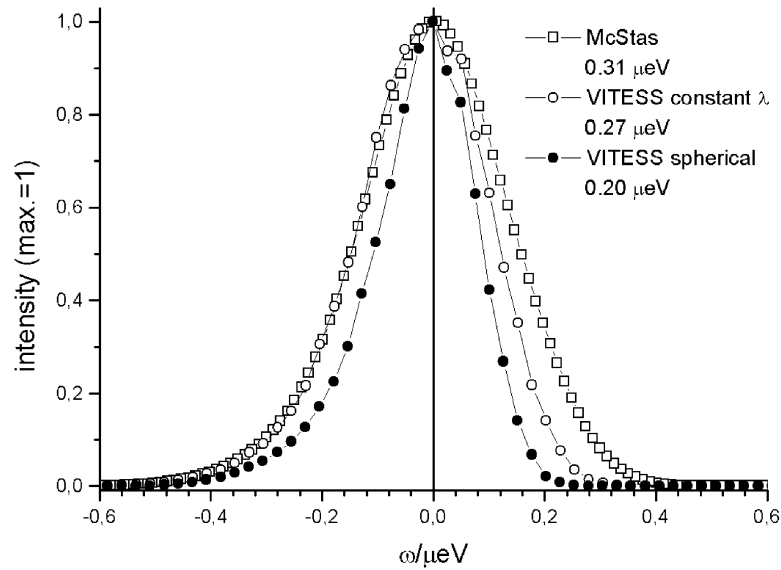


Fig. 5. The simulations using VITESS shows that the approximate spherical analyzer (closed circles) decreases the secondary flight time differences relative to the exact wavelength focussing (open circles). The comparison of the results obtained from the two packages, (VITESS—circles, MacStas—squares) shows that the resolution function is slightly asymmetric due to the tail on the moderator.

However due to the large bandwidth necessary (6.219 Å) for the performance of the instrument, this solution may not be viable. Another possibility is the use of a Drabkin filter, [7] where the basic idea is to create a resonance condition such that only neutrons having two selected parameter values (in time and in wavelength) will be transmitted. Neutrons that do not fulfill both conditions, for example those neutrons from the moderator tail, will not be reflected by the second mirror. After transmission through the energy filter, the wavelength–time relation will be much sharper than before. Another useful application of the device is that it will filter out the steady background of delayed neutrons, which are constantly emitted from the target or from activated shielding. However, this requires the use of a polarized neutron beam and a loss in neutron flux on sample of at least a factor of two.

## 5. Optimization of long-wavelength analyzers

Mica are aluminosilicate minerals with a sheet structure having two layers of silicate tetrahedra

arranged between a layer of hydrated metal-oxide octahedra, existing in different species such as muscovite, annite, phlogopite, fluoro-phlogopite and biotite. Slabs of single crystalline mica are of interest as a cold-neutron monochromators or analyzers in high-resolution spectrometers due to their large lattice spacing (about 10 Å). Recent investigations [8] of synthetic fluorinated mica, fluoro-phlogopite  $K_2Mg_6(AlSi_3O_{10})_2F_4$ , show strong (002) and (006) reflections and a weak (004) reflection with very low thermal diffuse scattering. Natural phlogopite,  $K_2Mg_6(AlSi_3O_{10})_2(OH)_4$ , show all reflections consistently strong with higher backgrounds. Fluorinated mica has the following unique characteristics: high chemical stability, excellent reflectivity, outgassing-free at high temperature in vacuum, excellent electrical insulation, high heat endurance (up to 1100°C), non-radioactive background, highly flexible and cleavable, which are much superior to that of natural mica. In addition, large fluorinated mica crystals of high quality can be grown by a Bridgman–Stockbarger method [9]. Given the lower background due to greatly reduced incoherent scattering, it is reasonable, despite the greater

price, to consider fluoro-phlogopite as an option. However, it is clear that optimization of the crystal analyzers is crucial to the operation of the spectrometer. Parameters such as neutron reflecting properties [10] and ideal crystal thickness must be fully explored.

## 6. Final remarks

The proposed 200 neV spectrometer (using the mica (002) reflection) offers a remarkable  $Q$ -range  $0.05 \text{ \AA}^{-1} \leq Q \leq 0.6 \text{ \AA}^{-1}$ , with a high  $Q$  resolution of  $0.002 \text{ \AA}^{-1} < \delta Q < 0.015 \text{ \AA}^{-1}$  and excellent dynamic range of  $-60 \text{ \mu eV} < \omega < 60 \text{ \mu eV}$ . Options include using higher order reflections to extend the ranges of both energy and momentum transfer. The LWTS will provide the high flux of long wavelength neutrons at the requisite pulse rate required by the spectrometer design.

MC computation using McStas and VITESS led to information on various properties for the proposed 200 neV spectrometer at LWTS, i.e. details on optimization of the guide system, effects of optical aberration, shape of the resolution function. In addition, based on the results of the MC simulations an interesting mode of operation for this spectrometer should be considered. One could run with one or more radial collimators of

varying acceptance and control the resolution of this instrument (much the way Soller collimators modify the resolution of a triple-axis spectrometer) and the corresponding intensity.

The complete set of SNS spectrometers, including the proposed LWTS neV instrument, will open unprecedented opportunities in the areas of chemical and biomolecular dynamics. Such studies often require systematic investigation of many similar molecules under slightly different conditions, requiring a large range of energy/timing resolutions for optimum study.

## References

- [1] SNS Long Wavelength Target Station Conceptual Design—NSF Proposal P-00106.
- [2] K. Lefmann, K. Nilesen, Neutron News 10/3 (1999) 20.
- [3] VITESS website: <http://www.hmi.de/projects/ess/vitess>.
- [4] G. Zsigmond, F. Mezei, D. Wechsler, F. Streffer, Nucl. Instr. and Meth. A 457 (2001) 299.
- [5] K.W. Herwig, Oak Ridge National Laboratory, ES-1.1.8.4-6017-RE-A-00, 1999, private communication.
- [6] C.J. Carlile, M.A. Adams, Physica B 182 (1992) 431.
- [7] Frank Klose, SNS design criteria for the SNS instrument systems magnetism reflectometer, 2001.
- [8] P. Allenspach, D. Engberg, PSI—focus progress report, 1998.
- [9] H.C. Pengdi Han, Materials Corporation, 1999, private communication.
- [10] M.L. Crow, Physica B 241–242 (1998) 110.